Wavelength-modulation laser hygrometer for ultrasensitive detection of water vapor in semiconductor gases

David Christian Hovde, Joseph T. Hodges, Gregory E. Scace, and Joel A. Silver

Water vapor is measured by use of a near-infrared diode laser and wavelength-modulation absorption spectroscopy. Humidity levels as low as 5 nmol/mol [1 nmol/mol = 1 ppb (1 ppb equals 1 part in 10^9)] of water vapor in air are measured with a sensitivity of better than 0.2 nmol/mol (3σ). The sensitivity, linearity, and stability of the technique are determined in experiments conducted at the National Institute of Standards and Technology, Gaithersburg, Maryland, by use of the low frost-point humidity generator over the range from 5 nmol/mol to 2.5 μmol/mol of water vapor in air. The pressure-broadening coefficients for water broadened by helium [0.0199(6) cm^{-1} atm^{-1} HWHM] and by hydrogen chloride [0.268(6) cm^{-1} atm^{-1} HWHM] are reported for the water line at 1392.5 nm.

1. Introduction

Measuring local concentrations of water vapor at mole fractions near nanomole-per-mole levels is important in many industrial applications,[1–3] especially the fabrication of semiconductors. Sensitive methods and instruments for measuring water vapor include atmospheric-pressure ionization mass spectrometry,[4] chilled-mirror hygrometers, electrolytic sensors,[2] mechanical microbalances, and capacitance sensors. Shortcomings of these existing approaches include high costs, slow response times, poorly characterized surface interactions, indirect calibration, or inability to measure moisture in hydrogen, oxygen, and condensible or corrosive gases.

Of the optical methods that have been applied to moisture measurement Fourier transform infrared (FTIR) spectroscopy[5] has the smallest dynamic range and the poorest sensitivity (~10 nmol/mol). Because water vapor is a component of room air, the entire FTIR spectroscopy optical path must be kept in an extremely dry enclosure, which adds significantly to its cost and complexity. Intracavity laser absorption spectroscopy is an extremely sensitive method for humidity sensing.[6] Unfortunately, it is difficult to calibrate, has a limited dynamic range, and requires additional work to make it rugged enough for routine industrial use. Cavity ring-down spectroscopy[7,8] has the potential for high precision and accuracy, but pulsed-laser sources remain costly and complex in the spectral regions of strongest water absorption. Sensitive single-mode cavity ring-down techniques based on locking cw lasers to high-finesse cavities may be able to approach the 0.01-nmol/mol sensitivity level.[7] Water vapor has been measured at nanomole-per-mole levels by use of lead-salt lasers,[9,10] but with their need for cryogenic cooling and frequent beam diagnostics lead-salt laser systems are more suited to laboratory experimentation than to commercial instrumentation.

We report a wavelength-modulation laser hygrometer (WMLH) for the ultrasensitive detection of water vapor.[11] For detecting H_2O this instrument combines wavelength-modulation absorption spectroscopy (WMS)[12–16] that uses near-infrared InGaAsP diode lasers near 1392.5 nm with a multipass absorption cell that is designed to minimize outgassing. Near-infrared lasers, originally developed for the communications industry, operate at room temperature to produce light with excellent spatial and spec-

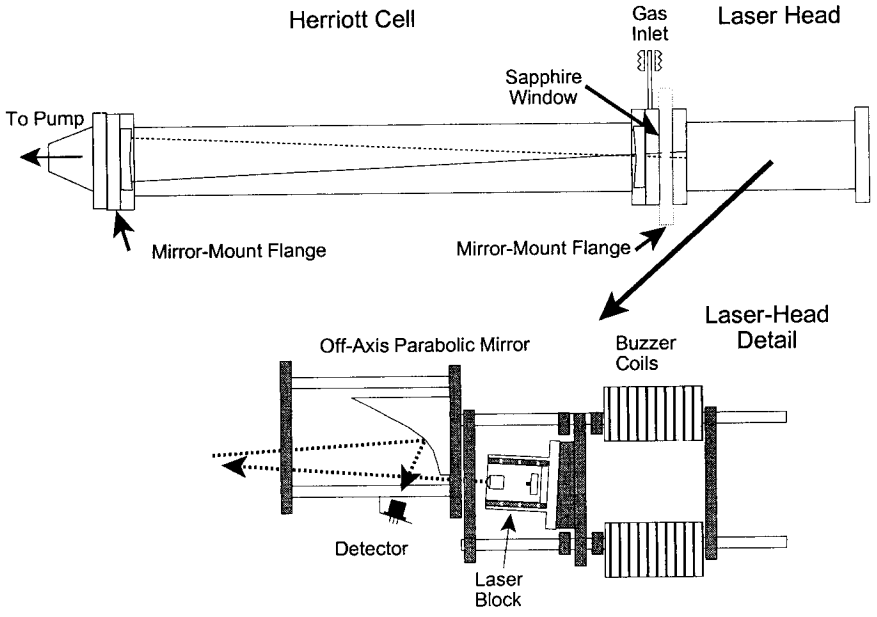

Fig. 1. Schematic of the WMLH (top) and detail of the laser-head assembly (bottom).

tral properties. The WMLH is applicable to corrosive as well as inert feed gases and has the desired combination of linearity, response speed, sensitivity, and accuracy. The water-vapor level derived from a detailed numerical model of the spectroscopic signal is compared with humidity levels in the range of 5 nmol/mol to 2.5 μmol/mol of water vapor in air and delivered by a stable thermodynamic source. The stability of the laser system is determined from the Allan variance of time series that is obtained during measurements of air containing 15 and 100 nmol/mol of water vapor. Pressure-broadening coefficients are reported for the 1392.5-nm water line[17] when broadened by He and HCl.

Other researchers have used near-infrared lasers to measure trace moisture levels in the nanomole-per-mole range. A near-infrared wavelength-modulation spectrometer for measuring water vapor in ammonia was recently reported by Wu *et al.*[18,19] Their setup utilizes a single-pass, dual-beam approach in which the signal from a dry reference cell is subtracted from a separate sample cell. A minimum detectable absorbance of $\sim 1.8 \times 10^{-7}$ was achieved, although the use of a single optical pass limited the sensitivity to 12 nmol/mol. A two-beam approach also was reported by Girard and Mauvais[20] with the reference beam used to cancel the moisture signal that arose from the purged beam path outside their multipass cell. A detection limit of 5 nmol/mol was reported in N_2 and other gases on the basis of measurements made over the range of 0–10,000 nmol/mol. In contrast to the previous research, the results reported in this study were achieved without the need for a reference detector and without continuously purging the external path.

2. Experimental Apparatus

The diode laser absolute moisture sensor measures the amount of water vapor by the quantification of the absorbance of a single rotational line within a vibrational-overtone band of water vapor. The line at 1392.5 nm is chosen for its combination of line strength, lack of known interfering absorbances, and availability of single-frequency, InGaAsP diode lasers that are based on distributed-feedback technology. Wavelength modulation is used to enhance the signal-to-noise ratio (SNR) in the absorption measurement by the reduction of the contribution of excess (laser) noise to the total noise current.[12–16] The laser wavelength or frequency ν is slowly ramped over the absorption line and simultaneously modulated at a frequency f with some modulation waveform $\nu_m(t)$ (e.g., sine, triangle, or square wave). The absorption signal is quantified by lock-in detection, in this case at twice the modulation frequency, $2f$. This technique improves the SNR by approximately 3 orders of magnitude[12] compared with direct absorption spectroscopy and results in an observed line shape that is roughly the second derivative of the transmission curve.[13–16] Under computer control a spectral scan of this $2f$ line shape is recorded. The water-vapor concentration is determined by linear least-squares fitting[21,22] of the resulting spectrum by use of a theoretical model described below. After every spectrum is measured (approximately once per minute) the water concentration is updated and displayed.

The sensor design is based on a sealed laser head that is connected to a Herriott[23,24] multipass cell (Fig. 1), both built from 11.75-cm-diameter (4.43-in.-diameter) ultrahigh-vacuum stainless-steel flanges

sealed with copper gaskets. The laser (Sensors Unlimited,[25] Model SU1392 DFB-CD) and the 1-mm-diameter InGaAs detector are housed in the laser head, and an antireflection-coated sapphire window permits the beam to enter and exit the Herriott cell. An electromagnet vibrates the diode-laser–aspheric-lens assembly (see details in Fig. 1) to reduce the detection of etalon fringes by approximately 2 orders of magnitude.[25,26] The Herriott cell consists of two 1-m-focal-length stainless-steel mirrors coated with diamond-machined nickel and separated by approximately 94 cm. The beam enters the cell through a slot cut in the mirror next to the laser head. The optical path length depends on the ratio of the focal length of the mirrors to the mirror separation.[23,24] For accommodating manufacturing tolerances in the focal length and the cell length the mirrors are mounted by use of three screws to permit translation along the optical axis as well as tip and tilt adjustment. The grooves necessary for constrained kinematic motion are machined directly into the back face of the stainless-steel mirror substrate, minimizing the number of parts wetted by the measurement gas. An off-axis parabolic mirror focuses the beam exiting the Herriott cell onto the detector.

The electronics include a computer for instrument control and data analysis, laser current and temperature controllers, laser modulation, detection, amplification, and demodulation electronics, mechanical modulation, and pressure measurement. The laser is controlled by an ILX Model LDC 3722 current controller with a general-purpose interface bus control for temperature-tuning the laser. The laser-frequency temperature-tuning rate as measured with a traveling-mirror wavemeter is -12 GHz/K, and the dc-current tuning rate is -1.04 GHz/mA. A typical spectrum scans across 21 GHz.

The magnitude of the current-tuning rate for the applied modulation is smaller than that of the dc figure given above because of the finite heat capacity of the laser and its mount.[26] Calibration of the modulation depth is accomplished by the overmodulation of a narrow spectral line and then the fitting of the resultant line shape by the adjustment of the modulation-depth parameters. When a spectral line is overmodulated the relative positions of the lobes are determined largely by the modulation depth; in this limit the line shape only weakly influences the separation of the lobes. The lobe separations are measured in terms of the frequency ramp (determined in terms of the known dc-current-tuning rate), which means that the modulation calibration is highly correlated with the scan calibration. The internal reproducibility of this method is estimated to be 3%. The modulation level used in this study was typically 902 MHz (baseline to peak).

Spectra are obtained by the step scanning of the laser current—hence the laser center frequency—over the absorption transition. The transmitted laser power is measured by a photodiode. A custom preamplifier separately amplifies the ac and the dc photocurrents. The $2f$ component of the ac photocurrent is measured by a true sine-wave lock-in amplifier, whereas the low-pass-filtered dc component is digitized by an auxiliary analog-to-digital converter on the lock-in amplifier. The ratio of these two quantities at each frequency step ν_i (for $i = 1, 2, \ldots$) constitutes the measured WMS spectrum. The main data-acquisition and data-fitting program continually scans the laser current and fits the resultant spectra. Typically, a spectrum is measured with approximately 90 equal laser-frequency steps in ~70 s, giving an effective update rate on the water-vapor concentration of ~0.015 Hz. A general-purpose interface bus provides the interfaces between the computer and both the lock-in amplifier (which includes the digital-to-analog converters) and to the laser temperature–current controller. A graphical user interface displays the measured spectrum superimposed on the best-fit spectrum and also displays a strip-chart-style graph of the measured water-vapor concentration. The results of the fit, including parameter values and uncertainties, are stored to a log file for later review.

The Herriott cell is evacuated by a corrosion-proof direct-drive mechanical pump, and the sample pressure is monitored with a capacitance diaphragm gage. Pressures are regulated manually and are typically maintained near 13.3 kPa (100 Torr). This pressure provides the optimum in balancing the signal strength, while keeping the line shape sufficiently narrow so that the full shape can be recorded within the somewhat limited wavelength-scan range of the laser.

Initial experiments conducted at Southwest Sciences, Inc., focused on the optimization of the SNR by measurement of the residual moisture in the boil-off from liquid nitrogen. The main source of noise arises from etalon fringes that are formed accidentally in the optical path. In the system described here there are two significant etalons: One has a small free spectral range (~69 MHz), corresponding to a path difference of 4 times the Herriott cell length. This etalon is suppressed by the application to the laser of an additional jitter modulation of approximately 90 MHz with the method of Cassidy and Reid.[27] (The 90-MHz jitter modulation slightly increases the effective linewidth of the laser; it is not applied for the pressure-broadening measurements and is neglected in the numerical model.) The second etalon has a larger free spectral range of 940 MHz, corresponding to an optical path difference of 32 cm. This difference is close to the round-trip distance from the laser to either the sapphire window or Herriott cell entrance mirror. This etalon is suppressed by a combination of vibrating the laser,[28,29] choosing a modulation depth for which this etalon is minimized (a 902-MHz baseline-to-peak modulation depth),[27] and blackening the back surface of the mirror and the metal parts near the window with a graphite slurry.

Quantitative measurements of water vapor in air are made by use of the new low frost-point humidity generator[30] (LFPG) at the National Institute of Stan-

dards and Technology (NIST) in Gaithersburg, Maryland. The LFPG saturates a CO_2-free stream of air with water vapor by means of flowing the air through an ice-coated channel that is maintained at constant temperature and pressure. Its output can be predicted from thermodynamic principles and under ideal conditions is independent of the gas flow rate. The mole fraction of water vapor in the gas stream exiting the LFPG is computed in terms of the temperature-dependent vapor pressure of hexagonal ice[31] and the measured total gas pressure. A small correction, the so-called enhancement factor, for nonideal mixing and nonideal gas effects is also applied.[32]

At the lowest humidity levels the fractional uncertainty (the 2-standard-deviation value) of the water-vapor mole fraction delivered by the LFPG is estimated to be $\leq$2%, a value that is dominated by uncertainty in the vapor pressure of the ice. Despite this systematic uncertainty, the LFPG-generated humidity level can be maintained at a constant value for weeks by active control of the LFPG-saturator temperature. In practice, long-term variations of less than 2 mK in the saturator temperature are realized, corresponding to a fractional change of 0.04% in the water-vapor mole-fraction levels produced for these tests. On the basis of the saturator's temperature range and stability the LFPG is expected to generate water-vapor mole fractions ranging from 4 mmol/mol to 3 nmol/mol with differential changes in its output as small as 10 pmol/mol. The high precision and the wide dynamic range of this generator facilitate the testing of the stability of the laser hygrometer over its full operational range. Also, the LFPG provides an independent method for calibrating the response of the laser hygrometer. This result can be compared with the first-principles calibration, which is based on spectroscopic and electronic gain factors.

A portion of the sample gas from the LFPG is metered into the laser-absorption cell by use of a critical-flow orifice. With this arrangement the flow rates through the two systems can be controlled independently. Approximately 2 m of 0.25-in. (0.63-cm) electropolished stainless-steel tubing is used to connect the output of the LFPG to the laser-absorption cell.

Separately, pressure-broadening measurements are made in ultrahigh-purity He (Mattheson, 99.999% pure) or in semiconductor-grade HCl gas (Mattheson, 99.995% pure). The moisture in these latter experiments arises from outgassing from the apparatus, resulting in water-vapor mole fractions that are estimated to be $\leq$10 μmol/mol, which is sufficiently low that the effects of self-broadening can be neglected in the analysis. The sample temperature for all measurements reported below is ~21 °C.

3. Analysis

Although diode-laser instruments have been calibrated based on determining the signal strength from a known quantity of gas or based on the method of standard additions,[9,20] it is also possible to calibrate the instrument on the basis of only the known optical path length and the spectroscopic and the electronic gain factors.[33] The spectroscopic parameters include the line strength of water, pressure-broadening (Lorentzian) and Doppler-broadening (Gaussian) line widths, the frequency at the line center, and the modulation depth of the laser.

The technique of WMS is well understood both theoretically and experimentally.[13–16] Because the diode-laser linewidth, which is usually less than ~50 MHz HWHM, is much narrower than the spectral linewidth, $\geq$500 MHz, the laser is assumed to probe the absorption line at a single frequency. The ratio of the modulation depth to the modulation frequency is much greater than unity, ensuring that the instantaneous laser frequency can be decomposed into the sum of a constant term (the optical frequency) plus a slowly varying term (corresponding to the low-frequency wavelength modulation). The instantaneous laser frequency is given by $\nu_i + \nu_m(t)$, where ν_i is the center frequency and $\nu_m(t)$ is the wavelength-modulation waveform (e.g., sine, triangle) of a characteristic frequency f.

For a Lorentzian line shape and sinusoidal modulation a closed-form solution for the WMS line shape exists.[34] However, at the reduced pressure that optimizes the signals in the WMLH $g(\nu)$ is modeled accurately by a Voigt function for which a closed-form solution to $g_{\mathrm{WMS}}(\nu)$ is not available. Additionally, it is desirable to evaluate the signals from arbitrary non-sinusoidal-modulation waveforms. Both cases require a numerical determination of the WMS line shape. The WMS line shape $g_{\mathrm{WMS}}(\nu)$ is found from the Voigt line shape[35] $g(\nu)$ by the computation of the instantaneous absorption line shape $g[\nu_i + \nu_m(t)]$ at each value of ν_i. One full cycle of the modulation waveform $\nu_m(t)$ is represented by 128 discrete steps. (If the modulation amplitude is large compared with the linewidth, more steps are required.) The resulting 128-point array is Fourier transformed; only the $2f$ component at the detection phase is retained as $g_{\mathrm{WMS}}(\nu_i)$.[16] Computing the line shape for a complete 90-point spectrum thus requires 90 × 128 evaluations of the Voigt function and 90 fast Fourier transforms.

The measured spectrum is related to the theoretical ratio of $2f$ to the dc photocurrent by

$$\frac{V_{2f}}{V_{\mathrm{dc}}} = \frac{G_{2f}\Re_{2f}}{G_{\mathrm{dc}}\Re_{\mathrm{dc}}}\frac{I_{2f}}{I_{\mathrm{dc}}}, \tag{1}$$

where V is the measured voltage, G is the frequency-dependent electronic gain (in volts per amperes), $\Re$ is the detector responsivity (in amperes per watts), and I is the transmitted laser power (in watts). We assumed that $\Re_{2f} = \Re_{\mathrm{dc}}$ for the fast photodiode used to detect the transmitted laser power, as is expected from its high bandwidth (35 MHz) and low stray capacitance (150 pF). Lock-in demodulation recovers the ac photocurrent signal at the demodulation frequency $2f$. Dividing this ac quantity by the dc photocurrent converts the $2f$ signal into a fractional

Table 1. Parameters Used to Compute Moisture Concentrations

Parameter	Formula	Value
Lorentz broadening[a]	$P \times 0.03050$ MHz/Pa	580 MHz
Doppler broadening	$3.581 \times 10^{-7}(T/M)^{1/2}\nu_0$	311 MHz
Line strength[a]	Not applicable	1.80×10^{-20} cm^2 cm^{-1} molecule^{-1}
Path length	50 passes × 93.3 cm/pass	4665 cm

[a]Values were taken from the HITRAN database[37] as computed for 21 °C.

change in transmitted laser intensity and thus accounts for changes in transmitted intensity that are due to misalignment, broadband absorption by impurities, or thermal changes in detector responsivity.

The Beer–Lambert law relates the concentration of water molecules n_{H_2O} in the sample volume to the observed intensity change passing through the sample. When the peak absorbance is sufficiently small that the linear form of the Beer law can be used the signal given by Eq. (1) is linearly proportional to the product of the line strength, the path length, and the water concentration (all of which are constant over the 20-μs modulation time scale) times the WMS spectral line shape $g_{WMS}(\nu_i)$. This linear relation between small changes in transmission and gas concentration permits the use of a linear least-squares analysis to determine the best estimate of the water concentration.

Two extensions are made to this simple model of the Beer law absorption. First, the fit includes a quadratic baseline to account for electronic or optical artifacts or both (including nonlinear laser or electronic responses, broad etalons, and distortions associated with the wings of adjacent lines). Second, the derivative of the WMS line shape, taken with respect to frequency, is included. This derivative models any small frequency mismatch between the theoretical and the experimental spectra. Thus the water-vapor concentration is found by an unweighted least-squares fitting of each measured spectrum to a model that comprises five vectors: the WMS demodulated Voigt line shape $g_{WMS}(\nu)$, the derivative of this demodulated line shape $dg_{WMS}(\nu)d\nu$, and the quadratic baseline B:

$$\frac{V_{2f}}{V_{dc}} = w_{H_2O}g_{WMS}(\nu) + w_{\Delta\nu}dg_{WMS}(\nu)/d\nu + w_B B. \quad (2)$$

The results of the unweighted least-squares fit include the five amplitude factors w, an estimate of the statistical uncertainty in each factor, and the correlations among factors. When the center frequencies of the observed and the theoretical spectral peaks overlap the water concentration is related to the fitting coefficient by

$$n_{H_2O} = w_{H_2O}\frac{G_{dc}}{SlG_{2f}}, \quad (3)$$

where S is the line strength and l is the optical path length. The Voigt computation[35] requires as input the Lorentzian broadening width, the Doppler width, the scan voltage-to-frequency conversion factor, and the baseline-to-peak modulation amplitude. The spectroscopic parameters for the fit are listed in Table 1. Measuring the Herriott cell pressure and temperature allows the mole fraction of the water vapor to be computed by use of Eq. (3) and the ideal-gas law.

The coefficient that multiplies the derivative of the line shape, $w_{\Delta\nu}$, is a measure of the frequency difference between the observed spectral peak and the theoretical peak and also is proportional to the amount of water vapor being measured. An integrating feedback loop is operated to drive the ratio $w_{\Delta\nu}/w_{H_2O}$ by the adjustment of the average laser current. In this manner the experimental peak is kept centered on the theoretical peak. Peak misalignment would otherwise result in a systematic underestimation of the water concentration. By keeping the loop gain low, one can achieve a good performance even for water-vapor mole-fraction levels near 5 nmol/mol for which the SNR is modest. Peak-shift errors are small after the instrument has warmed up. These errors are not expected to contribute significantly to the total measurement error. However, it is also possible to use $w_{\Delta\nu}$ to correct the estimated water-vapor concentration by use of a Taylor approximation.

The four principal assumptions in this implementation of the least-squares analysis are (1) the center frequency of the peak is properly identified, (2) the spectrum contains no extraneous structure that is not modeled by the quadratic background and the WMS line shape, (3) the absorbance is small enough that the linear form of the Beer–Lambert law can be used, and (4) the laser-frequency tuning varies linearly with the laser-diode current. Extensions of the computational treatment could include the explicit calculation of optically thick signals (for 1 nmol/mol and 13.3 kPa only approximately 5×10^{-6} of the laser power is absorbed at line center), corrections for deviations of the modulation waveform from an ideal sine wave and for the laser's dc tuning from linear, and corrections for the finite laser linewidth (resulting in a somewhat greater calibration accuracy at low pressure).

4. Results and Discussion

A. Measurements by Use of National Institute of Standards and Technology Traceable Standards

In the series of experiments performed at NIST the WMLH measured the water-vapor content of a sample gas produced by NIST's new LFPG[30] over the

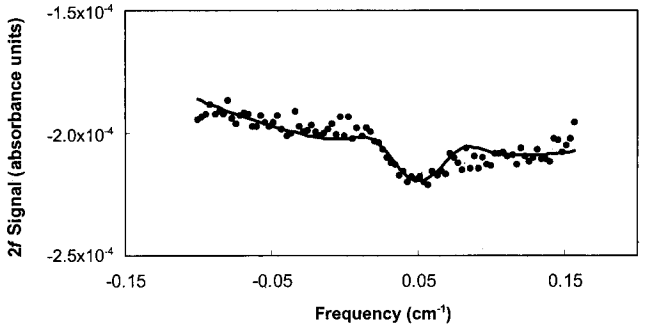

Fig. 2. Measured WMLH spectrum at 5 nmol/mol of water vapor in air (filled circles) converted from the raw lock-in amplifier/dc ratio to absorbance units and the fitted spectral data (curve).

range from 5 nmol/mol to 2.5 μmol/mol of water vapor in air. The WMS Voigt line shape is an excellent match to the observed signal, capturing 95% of the signal under high-SNR conditions. (The remaining mismatch may be due to the effects of amplitude modulation,[16] to nonlinear distortion of the modulation,[36] or to weak effects from additional lines in the spectrum.) At low moisture concentrations the deviation from the model is due to noise. A WMLH spectrum recorded at an expected LFPG water-vapor mole fraction of 5 nmol/mol is shown in Fig. 2 together with the curve representing the sum of the spectral-line and the background terms. The computed fractional absorbance at the line center that is due to water vapor is 2.9×10^{-5}. The ratio of the fitted signal to its standard deviation is 8.5. The rms sum of the residuals from a fit to this spectrum is 3.8×10^{-6} absorbance units. This low noise floor is achieved *without* the need to realign the laser after transporting it to NIST for these measurements.

Figure 3 shows a linear regression of all the inter-

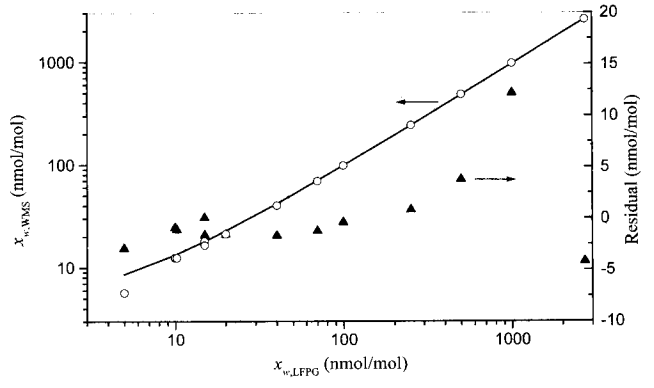

Fig. 3. Measured versus the generated water-vapor mole fraction: The open circles represent the spectroscopic determination of the water-vapor mole fraction by WMLH ($x_{w,WMS}$, left-hand coordinate) plotted versus the LFPG-generated mole fraction ($x_{w,LFPG}$) as predicted from the saturator temperature and pressure. The solid curve represents the linear fit to the WMLH data. The filled triangles (residual, right-hand coordinate) correspond to the WMLH measured value minus the predicted value of the water-vapor mole fraction for which the predicted values were based on the linear fit to the WMS data (curve).

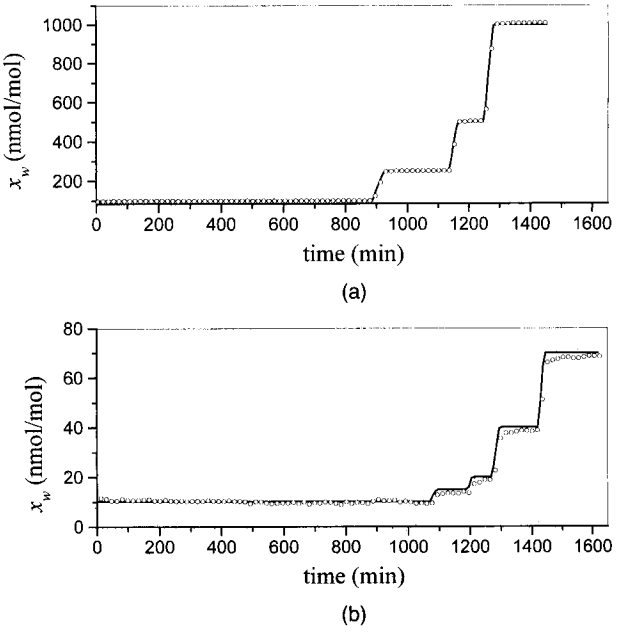

Fig. 4. Two time series of the LFPG expected output (solid curve) and the water-vapor mole fraction as measured by the WMS sensor (open circles).

comparison measurements, weighted by their observed variances, and the associated residuals. This intercomparison of the two instruments shows excellent agreement over the entire range studied with the difference between the two systems being consistent with the estimated uncertainties in the spectroscopic parameters as well as the vapor pressure of the ice. The fitting residuals are scattered about zero with a maximum value of less than 15 nmol/mol at the 2.5-μmol/mol point. These data exhibit good linearity and require only a 5% correction on the line-strength parameter, yet they indicate a small background level of ~3 nmol/mol. As is discussed below, this offset is attributed primarily to water-vapor outgassing effects that originate in the laser-absorption cell. These data were obtained over a span of several days during which time the system continued to dry out and background levels continued to decrease. Heating the Herriott cell to speed equilibration caused an unacceptable loss of optical alignment. It is interesting to note that, after exposure of the instrument to the atmospheric humidity, a period of only 1 day is required to reach a concentration of 10 nmol/mol.

Two time series that were obtained by stepwise changes in the LFPG set-point water-vapor mole fraction are illustrated in Fig. 4. The open circles correspond to the calibrated laser-hygrometer measurement, and the solid curve represents the expected LFPG output. These data illustrate the stability of both systems and reveal that the WMLH is capable of tracking relatively fast transients in the humidity level (e.g., factors of 2 in concentration on 20-min time scales). In Fig. 4(b) inspection of the WMLH data reveals a relatively slow reduction [~0.14 (nmol/mol)/hr] in the background level, and

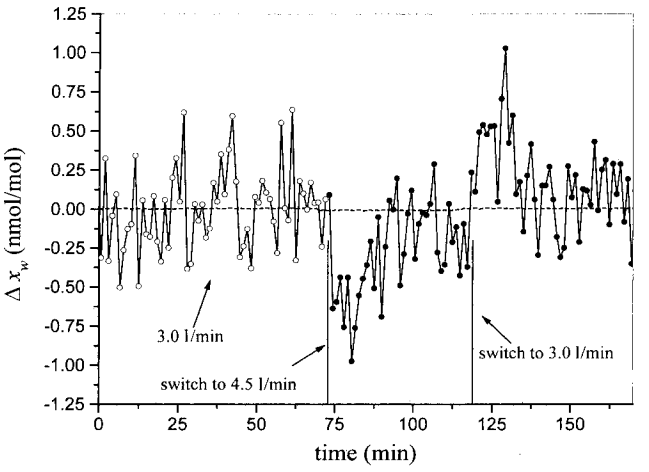

Fig. 5. Time series of the LFPG expected water-vapor mode fraction (dashed curve) and the WMS-measured water-vapor mole fraction (open and filled circles and solid curves). The flow rate through the LFPG was abruptly changed from 3.0 l/min to 4.5 l/min at $t \sim 70$ min and then set back to 3.0 l/min at $t \sim 120$ min. For this test the flow rate through the WMS sample volume was constant. The mole fractions are expressed as a difference from a representative mean value.

for LFPG set points of approximately 100 nmol/mol or below this suggests that equilibration of the WMLH response is rate limited by the outgassing of the water vapor. Outgassing effects in the laser hygrometer are investigated by variation of the volumetric flow rate Q through the cell in the range of 2 to 4 l/min. These tests were conducted at a fixed LFPG set-point water-vapor mole fraction. The background water-vapor level scales with Q^{-1}, a result that suggests that the background level is dominated by outgassing effects that occur within the Herriott cell and not in the laser-head assembly or the LFPG.

In a test of possible outgassing from the LFPG the gas flow rate through the LFPG was varied at a fixed LFPG saturator pressure and temperature, while keeping the flow rate through the WMLH constant. Under ideal conditions, the LFPG output is independent of the flow rate, and any observed change can be attributed to small changes in outgassing effects downstream of the generator or nonideal behavior of the LFPG saturator. Shown in Fig. 5 is the time response of the WMLH and the expected LFPG output. Prior to the changing of the flow rate the WMLH response exhibits a noise level of ~0.4 nmol/mol, a value that is consistent with calculated uncertainties in the spectral fits. After an increase in the flow rate in the LFPG from 3 to 4.5 l/min, the WMS response decreased by ~1 nmol/mol, and within 25 min it restabilized to an average value that was approximately 0.25 nmol/mol lower than the original value. After we reset the LFPG flow rate back to the original level the laser-diode device detected another ~1 nmol/mol transient (in the opposite direction) and eventually relaxed to the original mean value. These results show that the WMS device is capable of resolving subnanomole-per-mole changes in the water-vapor mole fraction on time scales of the order of 10 min. Further, the measurements suggest that the water-vapor concentration delivered by the LFPG exhibits a residual amount of flow-rate dependence. This weak effect is ascribed to outgassing in the flow system downstream of the LFPG.

The Allan variance[37,38] characterizes the WMLH noise as a function of the signal-averaging time. For each measurement ensemble, the LFPG set-point humidity level is allowed to equilibrate at a fixed value, and the WMLH-measured water-vapor mole fraction is recorded over an extended time interval. The results for two representative ensembles given by LFPG set-point water-vapor mole fractions of 15 and 100 nmol/mol [Figs. 6(a) and 6(b), respectively] are summarized in Fig. 6. Here the square root of the Allan variance is given as a function of the averaging time, and the corresponding distributions and Gaussian fits to these data are shown as insets. Both data sets exhibit nearly Gaussian distributions with standard deviations of ~0.4 nmol/mol. For both sets of data the Allan variance initially varies inversely with the averaging time, as is expected for Gaussian statistics. However, in Fig. 6(a) the square root of the Allan variance reaches a minimum value of ~65 pmol/mol for an averaging time of ~20 min, although still longer averaging times might have been possible had the system been fully equilibrated because it appears that the Allan variance at long averaging times is dominated by a slow trend toward drier conditions. In Fig. 6(b), outgassing effects are less important because of the relatively high water-vapor concentration in the sample gas, and no clear minimum in the WMLH Allan variance is observed for averaging times as long as 1 h. The standard deviation of the LFPG output mole-fraction data (calculated from the ensemble of the saturator's temperature and pressure measurements) is less than one tenth that of the WMS distribution, suggesting that the observed variations in the WMS measurement are not driven by temperature or pressure fluctuations occurring within the LFPG saturator.

From the Allan variance, one can evaluate the minimum detectable concentration and the resolution of the diode-laser absolute moisture sensor. The Allan variance also shows that the resolution and the minimum detectable concentration can be improved, but not without limit, by an increase in the averaging time. The minimum detectable concentration can be defined as the smallest signal that will produce a result that is statistically different from zero. Similarly, the instrument resolution can be defined as the smallest difference in sample concentration that is statistically significant. Inherent in these definitions is an assumption about statistical significance and about random noise in the measurements. Adopting a 3-standard-deviation criterion for statistical significance (99.7% confidence level) reveals the minimum detectable change in the mole fraction of the water vapor to be ~0.2 nmol/mol for averaging

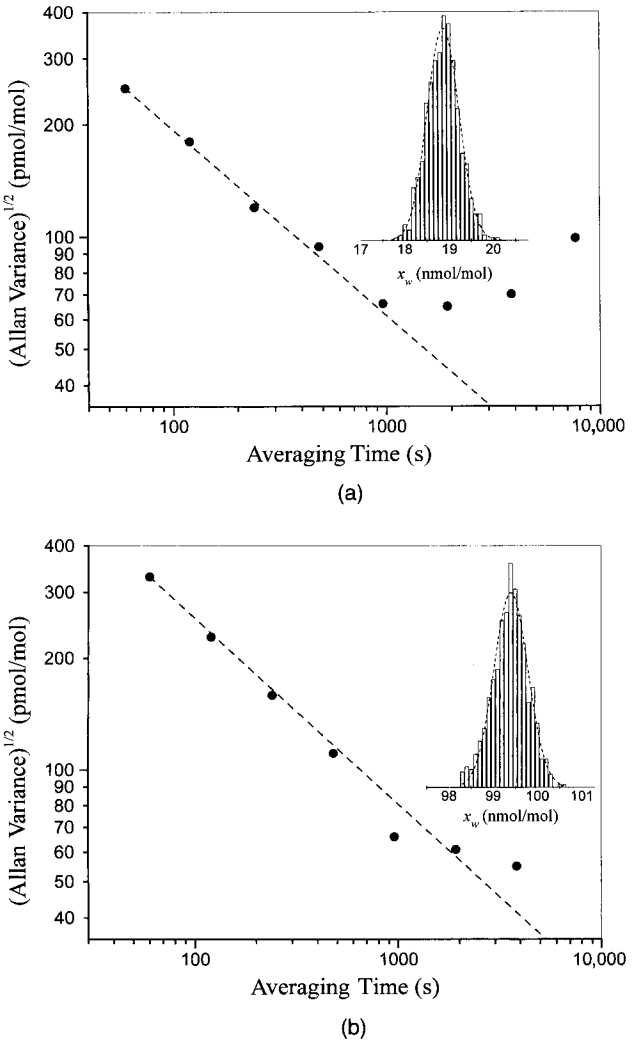

Fig. 6. Square root of the Allan variance (filled circles) plotted as a function of the averaging time for two time series that correspond to the WMS-measured mean water-vapor mole fractions of (a) 18.9 nmol/mol and (b) 100 nmol/mol. The dashed curves represent the expected decay in the Allan variance for fluctuations that obey stationary Gaussian statistics. Shown in the inset of each graph is the corresponding distribution and Gaussian fit of the observed mole fractions. Note that, in (a), the optimum averaging is approximately 1200 s and the square root of the Allan variance is approximately 65 pmol of water vapor per mole of air.

times of ~20 min. This result is consistent with those discussed for Fig. 5 from which a statistically significant change in the water-vapor mole fraction of $\gtrsim$0.25 nmol/mol (induced by the changing of the flow rate through the LFPG) can be observed.

A useful figure of merit for comparing the performance of absorption-measuring instruments is the noise-equivalent absorption (NEA), defined here as the minimum detectable absorption coefficient per square root of the data-acquisition rate. As such, the NEA is a species-independent quantity because it does not depend explicitly on the absorption cross section. On the basis of the results presented in Fig. 6 the NEA of the WMLH is $\approx 3.5 \times 10^{-9}$ cm^{-1}/Hz$^{1/2}$. Also, using a Herriott cell path length of l = 4665 cm and an integration time of 70 s (corresponding to one measurement of the water-vapor concentration) shows that this NEA figure is equivalent to an absorbance level of 2×10^{-6}. Figures 5 and 6, which are based on actual time-series measurements and the rates at which entire spectra are recorded and fitted to yield updated values of the water-vapor concentration, compare favorably with those obtained with other sensitive absorption methods.[7,8]

B. Sensitivity of the Fittings

Although the numerical fitting statistics provide estimates of the random uncertainties in the fit parameters (concentration, frequency shift, and baseline vectors), these uncertainties do not include systematic errors in the fixed parameters, such as the broadening coefficient of water or the modulation depth of the laser. To evaluate the sensitivity of the data-recovery algorithm to variations in the fixed parameters requires that the computed water concentration be determined for a range of pressure-broadening parameters, modulation amplitudes, scan rates, and second-order nonlinear wavelength tuning by use of a single spectral scan. Only the fit parameters are varied—the experimental data are held constant. For a nominal pressure-broadened half-width of 450 MHz, a Doppler width of 315 MHz, a scan rate of 214 MHz/mA, and a modulation amplitude of 903 MHz, the sensitivities are as follows:

- Increasing the pressure-broadened contribution to the line width by 4% increases the recovered concentration by 5%.
- Increasing the assumed scan rate by 4% increases the recovered water concentration by 2%.
- Increasing the modulation depth by 2% decreases the recovered water concentration by 2%.
- Adding a nonlinear modulation term to minimize the fitting error changes the best pressure-broadening coefficient but has little effect (0.2%) on the recovered water concentration at a constant pressure-broadening coefficient.

The result of these tests is to clarify that the pressure-broadening and the laser-tuning parameters need to be well characterized. The published value for broadening of the 1392.53-nm water line by air, b = 0.03050 MHz/Pa (0.1031 cm^{-1} atm^{-1}) HWHM, fits our spectral data to within 5%.[39] The remaining variance appears as an asymmetry of the line and may be explained by residual amplitude modulation of the diode laser.[16]

C. Broadening of the Water Line by Helium

To assess the performance of the WMLH in other process gases, one must know the pressure-broadening coefficient. When He is used as the carrier gas substantially narrower lines result. We use two methods to measure the linewidth in He at ambient temperature (21 °C). In the first method the direct-absorption spectrum of the water line is re-

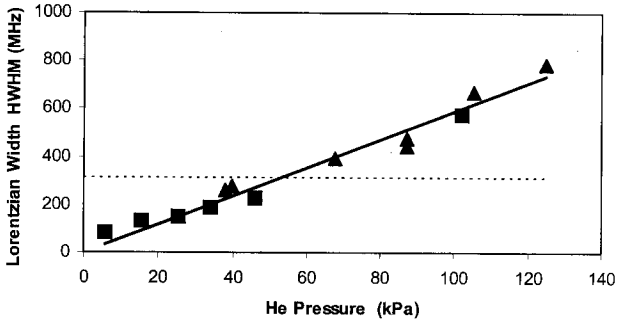

(a)

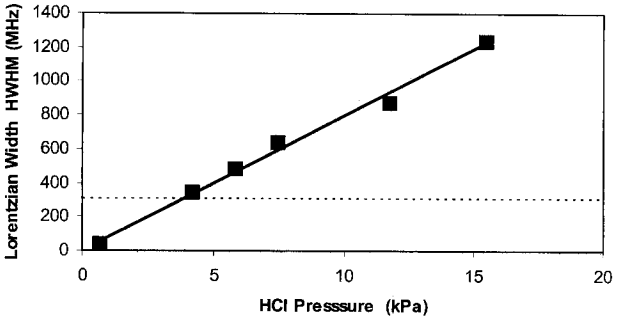

(b)

Fig. 7. Pressure-broadening measurement in He and HCl: (a) Dependence on He pressure of the Lorentzian component of the Voigt linewidth of the water transition[17] at 1392.53 nm as determined by WMS (squares) and by direct absorption (triangles). The solid curve represents a fit of all the data constrained to a zero intercept whose slope [5.8(2) kHz/Pa] is the He pressure-broadening coefficient. (b) Lorentzian component of the water transition plotted versus the HCl pressure as measured by direct absorption (squares). The solid curve is the same as for (a) but with a slope of 79(2) kHz/Pa. The dashed, horizontal lines in each graph indicate the Doppler HWHM.

corded as a function of the total pressure without modulating the laser. Using static samples of He causes outgassing to raise the water-vapor mole fraction to the 10-μmol/mol range, resulting in optically thick (>10% absorbance) signals. However, the water-vapor mole fraction is sufficiently small that self-broadening can be neglected when interpreting the data. The data analysis consists of manually optimizing the Lorentzian part of the linewidth and the line amplitude of the spectrum modeled as the ratio of a direct-absorption feature on a linear baseline function by use of a full-exponential Beer–Lambert law treatment. In the second method the water concentration is reduced by the flowing of He through the sample cell. Wavelength-modulation spectroscopy is used to record the resultant weaker absorption signals. The linear approximation to the Beer–Lambert law with the wavelength-modulation theory then is used to analyze the signals to determine the Lorentzian part of the linewidth.

The results of the above-described test are shown in Fig. 7(a). Good agreement is obtained between the two methods. Over the range from 1 to 120 kPa (0.01 to 1.2 atm) of He pressure the pressure-broadening coefficient of the $(1,0,1)2_{0,2} \leftarrow (0,0,0)3_{0,3}$ transition at 1392.53 nm (Ref. 17) is 5.8(2)-kHz/Pa [0.0199(6)-cm^{-1} atm^{-1}] HWHM, obtained by the fitting of the combined data set constrained to a zero intercept. Gamache *et al.*[40] summarized earlier microwave investigations of the $3_{1,3} \leftarrow 2_{2,0}$ rotational transition for which the room-temperature pressure-broadening measurements range from 0.0217(2) to 0.0220(22) cm^{-1} atm^{-1}. Lazarev *et al.*[41] reported a slightly higher value of 0.024(6) cm^{-1} atm^{-1} for the pressure-broadening coefficient of the $(0,0,0)5_{1,5} \leftarrow (1,0,3)4_{1,4}$ line of water by He. Those authors also discuss the theoretical computation of pressure broadening by rare gases and its dependence on the rotational states of the water molecule.

D. Broadening of the Water Line by Hydrogen Chloride

HCl was studied as a broadener of the 1392.53-nm water line because of its commercial importance in semiconductor manufacturing. These tests were constrained to measurements on static samples of HCl by the limitations of the laboratory system for handling hazardous gases. As a result, the measured moisture level was in the 10-μmol/mol range, and only direct-absorption scans are reported in Fig. 7(b). From a fitting of the Lorentzian contribution to the Voigt width, constrained to a zero intercept, the pressure-broadening parameter was determined to be 79(2)-kHz/Pa [0.268(6)-cm^{-1} atm^{-1}] HWHM, more than an order of magnitude greater than that of He. We are aware of only one other measurement of the HCl broadening coefficient. Inman and McAndrew[10] report a value of 0.15-cm^{-1} atm^{-1} HWHM for broadening by HCl of the $(0,0,0)3_{3,0} \rightarrow (0,1,0)2_{2,1}$ midinfrared water line at 6863.95 nm.

Although a direct measurement by wavelength modulation of trace moisture in HCl is not reported in this study, a reasonable estimation of the sensitivity for its measurement can be deduced as follows: The broadening coefficient is 2.6 times greater for HCl than for air, so the system pressure must be dropped by a factor of 2.6 to achieve the same line shape. The noise expressed as an absolute water concentration is then unchanged because the same modulation levels can be used and the same etalon fringes will limit sensitivity. However, as a mixing ratio (in nanomoles per mole), the noise will be 2.6 times higher. Such measurements of moisture in dry HCl therefore would be expected to show a Gaussian spread of 1.0 nmol/mol, provided the presence of HCl does not significantly alter the outgassing properties of the cell and does not introduce spectral interferences. In a similar fashion the sensitivity for detecting trace moisture in He can be estimated.

E. Reducing Interference from Water Vapor

The absorption line is so strong that residual moisture inside commercially sealed lasers (either 9-mm transistorlike cans with a window or fiber-pigtailed units) and detectors can overwhelm the trace signals from the Herriott cell. This residual moisture signal can be reduced by the removal of the laser, the de-

tector window, or both and the filling of the laser head with a pressurized ultradry inert gas, such as N_2 or CO_2.[11] The spectral features of the residual moisture are pressure broadened and present a broad curved background that is easily distinguished from the sharper, low-pressure lines in the Herriott cell.[42] This discrimination permits the achievement of a nanomole-per-mole or better sensitivity even if the residual humidity level in the head in the dry fill gas is a few micromoles per mole.

However, at nanomole-per-mole levels of moisture even this degree of care may not be sufficient. In addition to the above efforts the laser head is treated with D_2O vapor[43] to convert the adsorbed and the gas-phase water to a mixture of D_2O and HDO. The isotopic change shifts the absorption frequency away from the water line, although new spectral lines can be observed in the same region. In a separate 1-year test this method was found to be more effective at reducing the H_2O water-vapor signal than was the use of calcium sulfate desiccant. The efficacy of this passivation technique is also supported by the finding (reported above) that outgassing within the Herriott cell dominated the observed background levels.

F. Use of Different Modulation Waveforms

The numerical model is capable of accepting nonsinusoidal-modulation waveforms. The best signal–etalon ratio is obtained by use of a triangle-modulation waveform.[44] However, when the triangle-current waveform is applied to the laser the actual modulation that results is distorted because the wavelength tuning of the laser arises largely from temperature changes in the laser junction. The finite heat capacity and the thermal conductivity cause frequency-dependent phase and amplitude distortion of the wavelength modulation relative to the driving current.[26] Analysis of data that were collected by use of a triangle-modulation waveform indicated that the modulation was filtered by a combination of these thermal effects and the finite bandwidth of the laser-current driver. Because accurate calculation of WMS signals is possible only when the modulation is accurately known, either sinusoidal modulation should be used for quantitative work, a predistorted waveform must be used, or the triangle waveform must be carefully calibrated.

5. Conclusions

Measurements of the water-vapor concentration by use of the wavelength-modulation laser hygrometer have proved to be sensitive, precise, and accurate. Using a combination of methods to suppress etalons and achieve high SNR's achieved the best noise level achieved, which was equivalent to 65 pmol/mol in a 20-min averaging window. The three-sigma detection level, 195 pmol/mol, corresponds to a frost point of −120 °C. The linearity of the instrument is excellent, exhibiting an error of only 1% at water-vapor concentrations in the micromole-per-mole range (frost points near −65 °C). The most significant limitation on the accuracy appears to be from outgassing within the sample region.

In contrast to an atmospheric-pressure ionization mass spectrometer, the WMLH can be calibrated *a priori* on the basis of the measured spectral properties of water vapor, the laser-tuning characteristics, and the electronic gains. Good agreement is obtained with a precision moisture source over the range from 5 nmol/mol to 2.5 μm/mol. This method of calibration requires an accurate knowledge of the modulation waveform. A sine-wave–modulation waveform is expected to yield the highest fidelity and should give the most accurate results. Compared with a chilled-mirror hygrometer, the diode-laser sensor offers the advantages of a rapid time response and a direct gas-phase measurement with no ambiguity arising from the phase of the ice and its vapor pressure.

The sensitivity reported in this study is comparable to the near-infrared laser moisture measurements reported by Girard and Mauvais[20] and exceeds those obtained by Wu *et al.*[18,19] These comparisons have been achieved without a second reference path and without the need for continuous purging of the path external to the sample region. The data analysis is automated: moisture readings are updated after every spectrum. A simple line-locking method has been described.

Continued testing of the WMLH is planned. Possible experiments include the study of differential comparisons of the LFPG with other sources of humidity, the measurement of material outgassing rates following controlled moisture challenges, and other experiments for improved standards or materials science. This laser sensor can also serve as a prototype for an on-line diagnostic of feed gases used in semiconductor manufacturing.

We are grateful to James Whetstone at NIST for his role in enabling the WMS–LFPG intercomparison experiments. This study was funded by the U.S. Department of Commerce under contract 50-DKNB-5-00189.

References and Notes

1. J. Wei, J. E. Pillion, S. M. King, and M. Verlinden, "Using an in-line monitor to obtain real-time moisture measurements," MICRO Mag. 15, 31–36 (1997).
2. J. J. McAndrew and D. Boucheron, "Moisture analysis in process gas streams," Solid State Technol. **35,** 55–60 (1992).
3. S. A. Tison and J. P. Looney, "Workshop on water: its measurement and control in vacuum," J. Res. Natl. Inst. Stand. Technol. **100,** 75–83 (1995).
4. S. Ketkar, "Atmospheric pressure ionization mass spectrometry calibration and measurement of sub ppb levels of water in bulk gases," in *Proceedings of the NIST/AVS Workshop on Water: Its Measurement and Control in Vacuum* (National Institute of Standards and Technology, Gaithersburg, Md., 1994), pp. 22–23; see also Ref. 3.
5. B. R. Stallard, L. H. Espinoza, R. K. Rowe, M. J. Garcia, and T. M. Niemczyk, "Trace water vapor detection in nitrogen and corrosive gases by FTIR spectroscopy," J. Electrochem. Soc. **142,** 2777–2782 (1995).
6. G. Atkinson, "High sensitivity water detection: intracavity

laser spectroscopy," in *Proceedings of the NIST/AVS Workshop on Water: Its Measurement and Control in Vacuum* (National Institute of Standards and Technology, Gaithersburg, Md., 1994), pp. 44–45; see also Ref. 3.
7. B. A. Paldus, J. S. Harris, J. Martin, J. Xie, and R. N. Zare, "Laser diode cavity ring-down spectroscopy using acousto-optic modulator stabilization," J. Appl. Phys. **82,** 3199–3204 (1997).
8. R. D. van Zee, J. T. Hodges, and J. P. Looney, "Pulsed, single-mode cavity ring-down spectroscopy," Appl. Opt. **38,** 3951–3960 (1999).
9. J. A. Mucha, "Standard addition technique for quantitative trace gas analysis using derivative infrared diode laser spectroscopy," Appl. Spectrosc. **36,** 393–400 (1982).
10. R. S. Inman and J. J. F. McAndrew, "Application of tunable diode laser absorption spectroscopy to trace moisture measurements in gases," Anal. Chem. **66,** 2471–2479 (1994).
11. C. Hovde and J. A. Silver, "High sensitivity measurement of water vapor by tunable diode laser absorption spectroscopy," in *Proceedings of the NIST/AVS Workshop on Water: Its Measurement and Control in Vacuum* (National Institute of Standards and Technology, Gaithersburg, Md., 1994), pp. 47–48; see also Ref. 3.
12. D. S. Bomse, A. C. Stanton, and J. A. Silver, "Frequency modulation and wavelength modulation spectroscopies: comparison of experimental methods using a lead-salt diode laser," Appl. Opt. **31,** 718–731 (1992).
13. J. Reid and D. Labrie, "Second harmonic detection with tunable diode lasers—comparison of experiment and theory," Appl. Phys. B **26,** 203–210 (1981).
14. J. A. Silver, "Frequency modulation spectroscopy for trace species detection: theory and comparison among experimental methods," Appl. Opt. **31,** 707–717 (1992).
15. F. S. Pavone and M. Inguscio, "Frequency- and wavelength-modulation spectroscopies: comparison of experimental methods using an AlGaAs diode laser," Appl. Phys. B **56,** 118–122 (1993).
16. P. Kluczynski and O. Axner, "Theoretical description based on Fourier analysis of wavelength-modulation spectrometry in terms of analytical and background signals," Appl. Opt. **38,** 5803–5815 (1999).
17. The assignment listed by HITRAN (Ref. 37) for this transition is $(\nu_1\nu_2\nu_3)J_{Ka,Kc} = (0,0,0)3_{0,3} \rightarrow (1,0,1)2_{0,2}$.
18. S.-Q. Wu, J. Morishita, H. Masusaki, and T. Kimishima, "Quantitative analysis of trace moisture in N_2 and NH_3 gases with dual-cell near-infrared diode laser absorption spectroscopy," Anal. Chem. **70,** 3315–3321 (1998).
19. S.-Q. Wu, H. Masusaki, T. Kimishima, H. Kuze, and N. Takeuchi, "Absorption spectrometry of trace moisture in ammonia gas with a 1371-nm distributed-feedback diode laser," Jpn. J. Appl. Phys. Part 1 **38,** 4788–4793 (1999).
20. J.-M. Girard and P. Mauvais, "PPB-level hygrometry in nitrogen and ESG's using tunable diode laser spectroscopy," in *Proceedings of the International Symposium on Semiconductor Manufacturing '96* (Institute of Electrical and Electronic Engineers, New York, 1996), pp. 325–328.
21. R. D. May and C. R. Webster, "Data processing and calibration for tunable diode laser harmonic absorption spectrometers," J. Quant. Spectrosc. Radiat. Transfer **49,** 335–347 (1993).
22. A. Fried, B. Henry, and J. R. Drummond, "Tunable diode laser ratio measurements of atmospheric constituents by employing dual fitting analysis and jump scanning," Appl. Opt. **32,** 821–827 (1993).
23. D. Herriott, H. Kogelnik, and R. Kompfner, "Off-axis paths in spherical mirror interferometers," Appl. Opt. **3,** 523–526 (1964).
24. J. Altmann, R. Baumgart, and C. Weitkamp, "Two-mirror multipass absorption cell," Appl. Opt. **20,** 995–999 (1981).
25. Manufacturers and product names are given solely for completeness. These specific citations neither constitute an endorsement of the products nor imply that similar products from other companies would be less suitable.
26. A. Nadezhdinskii, "Diode laser frequency tuning," Spectrochim. Acta Part A **52,** 959–965 (1996).
27. D. T. Cassidy and J. Reid, "Harmonic detection with tunable diode lasers—two-tone modulation," Appl. Phys. Part B **29,** 279–285 (1982).
28. J. A. Silver and A. C. Stanton, "Optical interference fringe reduction in laser absorption experiments," Appl. Opt. **27,** 1914–1916 (1988).
29. J. A. Silver and A. C. Stanton, "Laser absorption detection enhancing method and apparatus," U.S. patent 4,934,816 (19 June 1990).
30. G. E. Scace, P. H. Huang, J. T. Hodges, D. A. Olson, and J. R. Whetstone, "The new NIST low frost-point humidity generator," in *Proceedings of the 1997 National Conference of Standards Laboratories: Workshop and Symposium* (National Conference of Standards Laboratories, 1800 30th Street, Suite 305B, Boulder, Co., 1997), pp. 657–673.
31. A. Wexler, "Vapor pressure formulation for ice," J. Res. Natl. Bur. Stand. Part A **81,** 5–19 (1977).
32. R. W. Hyland, "A correlation for the second interaction virial coefficients and enhancement factors for moist air," J. Res. Natl. Bur. Stand. Part A **79,** 551–560 (1975).
33. N. Goldstein, S. Aldergolden, J. Lee, and F. Bien, "Measurement of molecular concentrations and line parameters using line-locked second harmonic spectroscopy with an AlGaAs diode laser," Appl. Opt. **31,** 3409–3415 (1992).
34. R. Arndt, "Analytical line shapes for Lorentzian signals broadened by modulation," J. Appl. Phys. **36,** 2522–2524 (1965).
35. A. K. Hui, B. H. Armstrong, and A. A. Wray, "Rapid computation of the Voigt and complex error functions," J. Quant. Spectrosc. Radiat. Transfer **19,** 509–516 (1978).
36. V. G. Avetisov and P. Kauranen, "Two-tone frequency-modulation spectroscopy for quantitative measurements of gaseous species: theoretical, numerical, and experimental investigation of line shapes," Appl. Opt. **35,** 4705–4723 (1996).
37. D. W. Allan, "Statistics of atomic frequency standards," Proc. IEEE **54,** 221–230 (1966).
38. The Allan variance calculation was made by use of the LabView computer program SRAV.VI, written by D. Moschella and downloaded from ftp://ftp.pica.army.mil/pub/labview/vi/.
39. L. S. Rothman, C. P. Rinsland, A. Goldman, S. T. Massie, D. P. Edwards, J.-M. Flaud, A. Perrin, C. Camy-Peyret, V. Dana, J.-Y. Mandin, J. Schroeder, A. McCann, R. R. Gamache, R. B. Wattson, K. Yoshino, K. V. Chance, K. W. Jucks, L. R. Brown, V. Nemtchinov, and P. Varanasi, "The HITRAN molecular spectroscopic database and HAWKS (HITRAN atmospheric workstation): 1996 edition," J. Quant. Spectrosc. Radiat. Transfer **60,** 665–710 (1998); *HITRAN 1996* (Ontar Corp., 9 Village Way, North Andover, Mass. 01845-2000, 1996).
40. R. R. Gamache, R. Lynch, and L. Brown, "Theoretical calculations of pressure broadening coefficients for H_2O perturbed by hydrogen or helium gas," J. Quant. Spectrosc. Radiat. Transfer **56,** 471–487 (1996).
41. V. V. Lazarev, Yu. N. Ponomarev, B. Sumpf, O. Fleischmann, J. Waschull, H.-D. Kronfeldt, and V. N. Stroinova, "Noble gas pressure-induced broadening and shift of H_2O and SO_2 absorption lines," J. Mol. Spectrosc. **173,** 177–193 (1995).
42. J. A. Mucha and L. C. Barbalas, "Infrared diode laser determination of trace moisture in gases," ISA Trans. **25,** 25–30 (1986).
43. D. C. Hovde, D. J. Kane, and J. A. Silver, "Process for reducing interfering signals in optical measurements of water vapor," U.S. patent 5,804,702 (8 September 1998).
44. T. Iguchi, "Modulation waveforms for second-harmonic detection with tunable diode lasers," J. Opt. Soc. Am. B **3,** 419–423 (1986).